Available online at www.sciencedirect.com

SciVerse ScienceDirect

Ceramics International 39 (2013) 1597–1602

CERAMICS INTERNATIONAL

www.elsevier.com/locate/ceramint

Improvement of textured $Bi_{1.6}Pb_{0.4}Sr_2Co_{1.8}O_x$ thermoelectric performances by metallic Ag additions

A. Sotelo[a], Sh. Rasekh[a], G. Constantinescu[a], M.A. Torres[b], M.A. Madre[a,*], J.C. Diez[a]

[a]Instituto de Ciencia de Materiales de Aragón, CSIC-Universidad de Zaragoza, María de Luna 3, 50018 Zaragoza, Spain
[b]Departamento de Ingeniería de Diseño y Fabricación, Universidad de Zaragoza, María de Luna 3, 50018 Zaragoza, Spain

Received 11 July 2012; received in revised form 31 July 2012; accepted 31 July 2012
Available online 9 August 2012

Abstract

$Bi_{1.6}Pb_{0.4}Sr_2Co_{1.8}O_x$ thermoelectric ceramics with small Ag additions (0, 1, and 3 wt%) have been successfully grown from the melt, using the laser floating zone method. Microstructure has shown a reduction in the amount of secondary phases and a better grain alignment with respect to the growth direction for an Ag content of 3 wt%. The microstructural evolution, as a function of Ag content, is confirmed with the electrical resistivity values, which show an important decrease for the 3 wt% Ag samples, leading to maximum power factor values of about 0.42 mW/K^2 m at 650 °C, which are among the best results obtained in this type of material.

Keywords: A. Grain growth; B. Platelets; Microstructure-final; C. Electrical properties

1. Introduction

Thermoelectric (TE) materials with high energy conversion efficiencies are strongly required for electric power generation. Thermoelectric energy conversion is now showing very important advantages to harvest waste heat in a wide number of applications. Moreover, it can transform solar energy into electricity at lower cost than photovoltaic energy [1]. The conversion efficiency of such materials is quantified by the dimensionless figure of merit ZT, which is defined as $TS^2/\rho\kappa$ (in which S^2/ρ is also named power factor, PF), where S is the Seebeck coefficient (or thermopower), ρ the electrical resistivity, κ the thermal conductivity, and T is the absolute temperature [2]. As higher ZT means higher efficiency, an adequate TE material for practical applications must involve high thermopower and low electrical resistivity, with low thermal conductivity.

The discovery of large thermoelectric power in Na_xCoO_2 [3], which was found to possess a high ZT value of about 0.26 at 300 K, has opened a broad research field and from that moment on, great efforts have been devoted to explore new cobaltite families with high thermoelectric performances. Some other layered cobaltites, such as misfit $[Ca_2CoO_3][CoO_2]_{1.62}$, $[Bi_{0.87}SrO_2]_2[CoO_2]_{1.82}$ and $[Bi_2Ca_2O_4][CoO_2]_{1.65}$ were also found to exhibit attractive thermoelectric properties [4–8]. The crystal structure is composed of two different layers, with the alternate stacking of a common conductive CdI_2-type CoO_2 layer with a two-dimensional triangular lattice and a block layer, composed of insulating rock-salt-type (RS) layers. Both sublattices (RS block and CdI_2-type CoO_2 layer) possess common a- and c-axis lattice parameters and β angles but different b-axis length, causing a misfit along the b-direction [9–11].

As layered cobaltites are materials with a strong crystallographical anisotropy, the alignment of plate-like grains by mechanical and/or chemical processes is necessary to attain macroscopic properties comparable to those obtained on single crystals. Some techniques have been shown to be adequate to obtain a good grain orientation in several oxide ceramic systems, such as template grain

*Correspondence to: Departmento de Ciencia de Materiales, C/María de Luna 3, 50018 Zaragoza, Spain. Tel.: +34 976762617; fax: +34 976761957.
E-mail address: amadre@unizar.es (M.A. Madre).

0272-8842/$ - see front matter © 2012 Elsevier Ltd and Techna Group S.r.l. All rights reserved.
http://dx.doi.org/10.1016/j.ceramint.2012.07.112

growth (TTG) [10], sinter-forging [12], spark plasma [13], and directional growth from the melt [14]. On the other hand, it is interesting to explore cationic substitutions in the RS layer, which can change the misfit relationship between these two layers and, as a consequence, modify the values of the thermopower [7]. From this point of view, it is clear that this kind of substitution can be useful in order to improve thermoelectric performances of ceramic materials [12], as is reported for the substitution of Gd and Y for Ca [15], or Pb for Bi [16]. Moreover, metallic Ag additions have also been shown to improve, in an important manner, the mechanical and thermoelectrical properties of this system [17] and other similar materials [18] which nearly do not react with Ag.

Taking into account these previously discussed effects, the aim of this work is producing high performance TE materials by the addition of metallic Ag to the optimally Pb doped Bi–Sr–Co–O compound [16,19], followed by a texturing process performed by the laser floating zone (LFZ) technique.

2. Experimental

The initial $Bi_{1.6}Pb_{0.4}Sr_2Co_{1.8}O_x$ with small amounts of silver (0, 1, and 3 wt% Ag) polycrystalline ceramics were prepared from commercial $Bi(NO_3)_3 \cdot 5H_2O$ ($\geq 98\%$, Aldrich), $SrCO_3$ (98.5%, Panreac), $Co(NO_3)_2 \cdot 6H_2O$ (98%, Panreac), and metallic Ag (99%, Aldrich) powders by a sol–gel via nitrates method. They were weighed in the appropriate proportions and suspended in distilled water. Concentrated HNO_3 (analysis grade, Panreac) was added dropwise into the suspension until it turned into a clear pink solution. Citric acid (99.5%, Panreac), and ethylene glycol (99%, Panreac), were added to this solution in adequate proportions. Evaporation of the solvent was performed slowly in order to decompose the excess nitric acid, which allowed the polymerisation reaction between ethylene glycol and citric acid, forming a pink gel [20,21]. The dried product was then decomposed (slow self combustion) by heating at 350–400 °C for 1 h. The remaining powder was mechanically ground and calcined at 750 and 800 °C for 12 h, with an intermediate grinding. This step is especially important when texturing is performed using the LFZ technique: it has been designed to decompose the alkaline-earth carbonates which, otherwise, would decompose in the molten zone disturbing the solidification front. The so-obtained powders were cold isostatically pressed in the form of cylinders (~120 mm long and 2–3 mm in diameter) under an applied pressure of about 200 Mpa for 1 min.

The green ceramic cylinders were subsequently used as feed in a LZF texturing system used successfully in previous works [22–24] and described in detail elsewhere [25]. On the other hand, the growth rate has been chosen taking into account previous results obtained in layered ceramic samples [26,27]. As a consequence, all samples were grown downwards at 15 mm/h, with a seed rotation of 3 rpm, in order to maintain the cylindrical geometry in the final textured material, while the feed was rotated at 15 rpm in the opposite direction, to improve the molten zone homogeneity. After the texturing process, long (more than 150 mm) cylindrical and geometrically homogeneous samples were obtained. These textured materials were then cut into shorter pieces of adequate sizes for their characterisation (~15 mm long).

The structural identification of all the samples was performed by powder XRD utilising a Rigaku D/max-B X-ray powder diffractometer (CuKα radiation) with 2θ ranging between 10° and 70°. Microstructural observations were performed on polished samples using a field emission scanning electron microscope (FE-SEM, Carl Zeiss Merlin) fitted with energy dispersive spectrometry (EDS) analysis. Micrographs of these samples have been recorded to analyse the different phases and their distribution. From these pictures, an estimation of the amount of the different phases has been made using the Digital Micrograph software.

Steady-state simultaneous measurements of resistivity and thermopower were determined by the standard dc four-probe technique in an LSR-3 apparatus (Linseis GmBh) between 50 and 650 °C under a He atmosphere. From these data, PF values as a function of temperature were calculated in order to evaluate the final sample performances.

3. Results and discussion

Powder XRD patterns for all $Bi_{1.6}Pb_{0.4}Sr_2Co_{1.8}O_x$ samples with different amounts of Ag are plotted (from 10° to 40° for clarity) in Fig. 1. They show very similar patterns where the most intense peaks correspond to the misfit cobaltite $Bi_{1.6}Pb_{0.4}Sr_2Co_{1.8}O_x$ phase, in agreement with previous reported data [16,28]. From this figure, it is clear that the cobaltite phase appears as the major one, independently of Ag content. Peaks marked with a ● in the plot correspond to the Co-free $Bi_{0.75}Sr_{0.25}O_{1.375}$ secondary phase [29]. Moreover, for samples with 1 and 3 wt% Ag, a new peak appears in the XRD plots at around 38°, which corresponds to the metallic Ag (111) plane (indicated by ■) [30]. This peak also indicates that Ag does not react with the thermoelectric ceramic, leading to the formation of a ceramic matrix composite with metallic particles distributed inside the matrix, as observed in similar ceramic systems [18,27,31].

Scanning electron microscopy has been performed on polished longitudinal sections of all samples after the growth process. The microstructural evolution of samples, as a function of Ag content, can be easily observed in Fig. 2 where representative micrographs of longitudinal polished sections of all samples are presented. In these general views, it can be clearly seen that all samples are composed by three contrasts which correspond to different phases, identified by EDS and numbered, for clarity, in Fig. 2a. Grey contrast (#1) corresponds to the thermoelectric $Bi_{1.6}Pb_{0.4}Sr_2Co_{1.8}O_x$

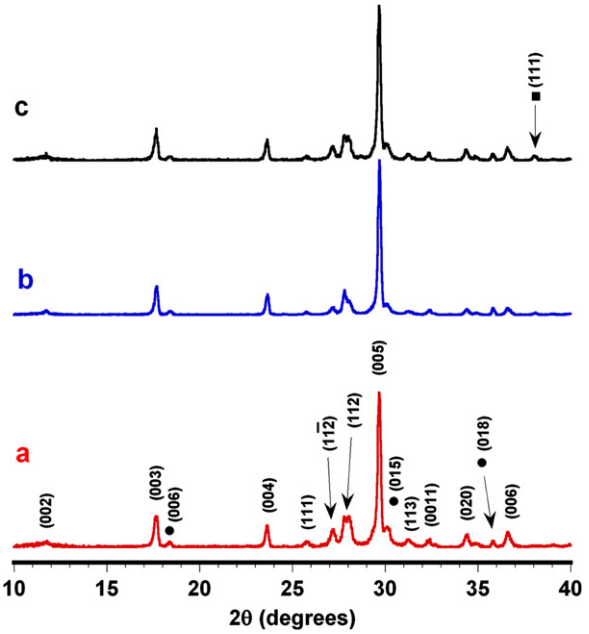

Fig. 1. Powder XRD diagrams for the $Bi_{1.6}Pb_{0.4}Sr_2Co_{1.8}O_x$ textured samples with (a) 0; (b) 1; and (c) 3 wt% Ag. Crystallographic planes have been indicated on the peaks corresponding to the $Bi_{1.6}Pb_{0.4}Sr_2Co_{1.8}O_x$ phase. Other phases are indicated by symbols: ● Co-free $Bi_{0.75}Sr_{0.25}O_{1.375}$ secondary phase; and ■ Ag.

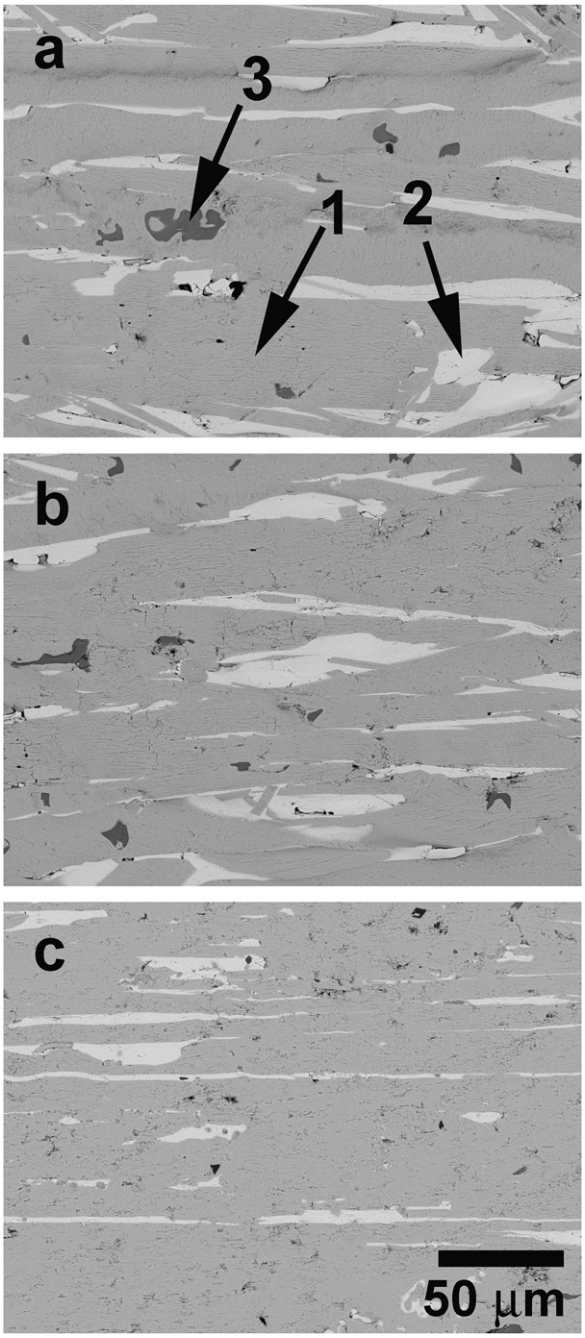

Fig. 2. Scanning electron micrographs from longitudinal polished textured samples $Bi_{1.6}Pb_{0.4}Sr_2Co_{1.8}O_x$ with different Ag contents: (a) 0; (b) 1; and (c) 3 wt%. The different phases are indicated by arrows: (1) $Bi_{1.6}Pb_{0.4}Sr_2Co_{1.8}O_x$; (2) $Bi_{2.2}SrO_y$; and (3) $SrCoO_z$.

phase, and white (♯2) and dark grey (♯3) ones to the $Bi_{2.2}SrO_y$ and $SrCoO_z$ secondary phases, respectively, which is in agreement with the previously discussed XRD data. Moreover, it can be observed that the amount and size of these secondary phases is reduced when the Ag content is increased. The approximate content of these secondary phases is about 14 vol% of $Bi_{2.2}SrO_y$ and 1.5 vol% of $SrCoO_z$ for the pure samples, which are reduced to around 12 and 1.3 vol% for the 1 wt%Ag ones, and 7 and 0.5 vol% found in the 3 wt%Ag samples.

Another interesting feature that can be observed in this figure is the $Bi_{2.2}SrO_y$ change in shape, from thick and relatively short grains in the pure $Bi_{1.6}Pb_{0.4}Sr_2Co_{1.8}O_x$ samples, to thinner and better aligned grains with respect to the growth direction when Ag is added. The reduction in thickness and good alignment of this secondary phase increases the effective area of the thermoelectric phase. This effect, together with an improved alignment of the thermoelectric phase, leads to the raise of transport properties.

On the other hand, Ag is not easy to see in the micrographs displayed in Fig. 2 due to their low magnification. In order to observe the Ag shape and distribution, higher magnification micrographs have been recorded for samples with 3 wt% Ag, and presented in Fig. 3a. In this micrograph, some Ag particles are indicated by arrows for clarity, as they show a very similar contrast to that of the thermoelectric phase. Furthermore, some regions with an eutectic-like microstructure can also be observed in Fig. 3a, surrounded by a broken line. This marked zone has been enlarged and displayed in Fig. 3b, where a homogeneous distribution of metallic Ag spherical particles in a $Bi_{1.6}Pb_{0.4}Sr_2Co_{1.8}O_x$ thermoelectric ceramic matrix can be clearly seen. This result is in agreement with previously reported works in similar ceramic materials which do not react with Ag but produce an eutectic detected experimentally by DTA analysis but not observed microstructurally before [32].

The temperature dependence of the electrical resistivity as a function of the Ag content is presented in Fig. 4. As can be easily seen, the $\rho(T)$ curves show very similar behaviour for samples with 0 and 1 wt% Ag, with only a

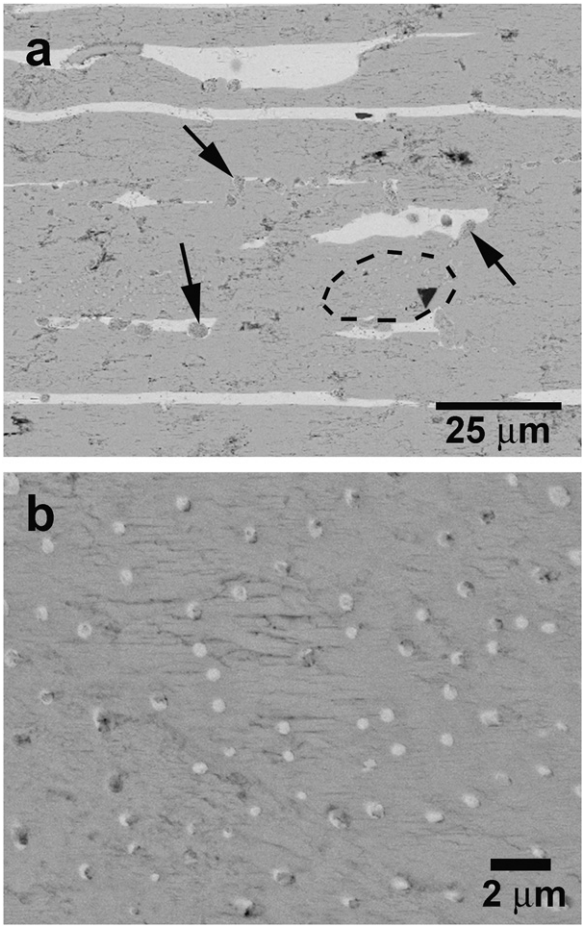

Fig. 3. Scanning electron micrographs from longitudinal polished samples $Bi_{1.6}Pb_{0.4}Sr_2Co_{1.8}O_x$ with 3 wt% Ag. Ag particles are indicated by arrows in (a). Broken line indicates the zone represented in (b), where an eutectic-like structure can be distinguished (Ag particles in a $Bi_{1.6}Pb_{0.4}Sr_2Co_{1.8}O_x$ phase matrix).

slight reduction in resistivity for the samples with 1 wt% Ag. Both curves display a semiconducting-like behaviour ($d\rho/dT < 0$) from room temperature to about 550 °C and a metallic-like one ($d\rho/dT > 0$) at higher temperatures. On the other hand, samples with 3 wt% Ag additions reduce the resistivity values significantly and change their behaviour radically showing a metallic-like one ($d\rho/dT > 0$) in all measured temperature ranges. This important reduction of electrical resistivity is consistent with the reduction of the secondary phase content already mentioned in the microstructure discussion (see Fig. 2) and the higher grain alignment, which has also been observed in similar ceramic systems [17,31]. The minimum resistivity value at room temperature, ~7 mΩ cm, is obtained for samples with 3 wt% Ag, while for the 0 and 1 wt% Ag it is about two times higher, 13 and 12 mΩ cm, respectively. In any case, these values are lower than those obtained in pure $Bi_{1.6}Pb_{0.4}Sr_2Co_{1.8}O_x$ processed by the same technique with higher growth speed [16]. Moreover, the minimum value is comparable to that obtained in single crystals with similar composition without Ag [33].

Fig. 5 displays the variation of the Seebeck coefficient as a function of temperature for all the samples. In this figure, it is clear that the sign of the Seebeck coefficient is positive for the whole measured temperature range, which confirms a conduction mechanism predominantly governed by holes. The values increase with temperature, with a slight change in the curve slope at about 300 °C for all the samples. Moreover, the room temperature values are very similar for the 0 and 1 wt% Ag samples while it is lower for the 3 wt% Ag samples, which is in agreement with the room temperature values of resistivity. In all cases, these room temperature values are higher than those measured in single crystals with similar composition without Ag (about 100 μV/K) [33]. The reason for obtaining such high values is the formation of considerable amounts of oxygen

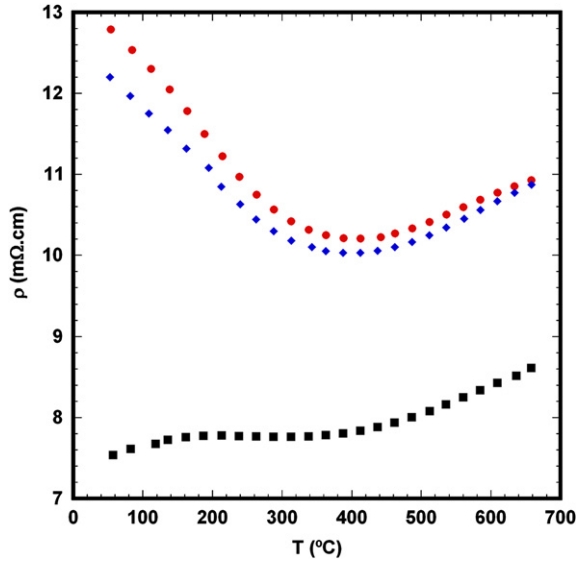

Fig. 4. Temperature dependences of the electrical resistivities for textured $Bi_{1.6}Pb_{0.4}Sr_2Co_{1.8}O_x$ with different Ag contents: ● 0; ◆ 1; and ■ 3 wt%.

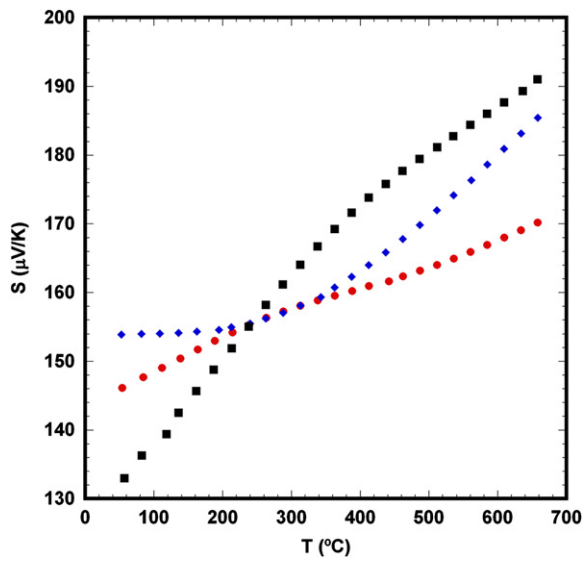

Fig. 5. Temperature dependences of the Seebeck coefficients for textured $Bi_{1.6}Pb_{0.4}Sr_2Co_{1.8}O_x$ with different Ag contents: ● 0; ◆ 1; and ■ 3 wt%.

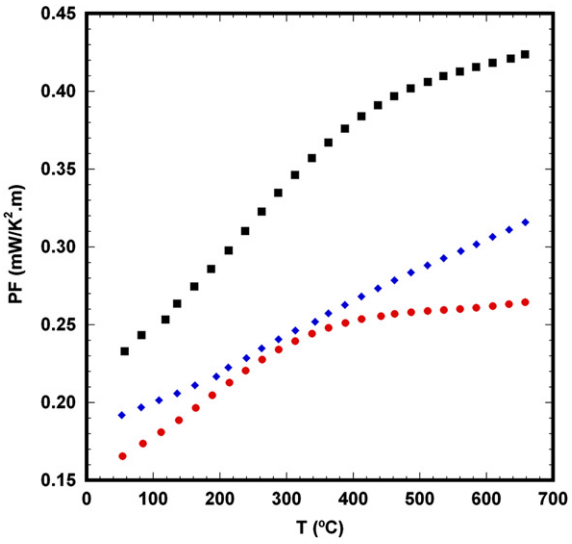

Fig. 6. Temperature dependences of the power factors for textured $Bi_{1.6}Pb_{0.4}Sr_2Co_{1.8}O_x$ with different Ag contents: ● 0; ◆ 1; and ■ 3 wt%.

vacancies on the thermoelectric phase when samples are textured using the LFZ technique [22]. This effect has also been observed in the misfit phase $[Ca_2CoO_3][CoO_2]_{1.62}$ which contains considerable amounts of oxygen vacancies when it is thermally treated under a reducing atmosphere [34]. The rise in oxygen vacancies changes the Co oxidation state from Co^{4+} to Co^{3+}, thus increasing S values, in agreement with the Koshibae equation [35].

In order to evaluate the thermoelectric performances of the textured ceramic materials, variation of the power factor with temperature has been calculated from the resistivity and Seebeck coefficient values and displayed as a function of the Ag content in Fig. 6. As was found in the resistivity and Seebeck factor measurements, samples with 0 and 1 wt% Ag show very similar values with a minimum value, at room temperature, of about $0.16\,mW/K^2\,m$, higher than the obtained values in single crystals with similar composition to the pure one ($\sim 0.14\,mW/K^2\,m$) [33]. Moreover, it is about 50% higher than that obtained for the pure $Bi_{1.6}Pb_{0.4}Sr_2Co_{1.8}O_x$ material processed by the LFZ technique at higher growth speeds [16]. On the other hand, samples with 3 wt% Ag additions increase the power factor values, at room temperature, in around 50% of the obtained values in Ag-free samples. This result indicates that small Ag additions can be very useful in order to strongly reduce electrical resistivity and, as a consequence, raises the thermoelectric performances.

The maximum PF value obtained in these samples, $\sim 0.42\,mW/K^2\,m$, is among the best results obtained in this type of materials so far, making them good candidates for application in practical thermoelectric devices.

4. Conclusions

This paper demonstrates that $Bi_{1.6}Pb_{0.4}Sr_2Co_{1.8}O_x$ thermoelectric materials with small Ag additions (0, 1, and 3 wt%) can be directionally grown by the laser floating zone method. It has been determined that the optimal Ag content in the textured materials is 3 wt%. Microstructural evolution shows that this amount of Ag reduces significantly the amount of secondary phases and induces their alignment with the growth direction. Moreover, the electrical resistivity data clearly indicated that this Ag amount simultaneously enhances the metallic behaviour of samples, together with an important reduction of their resistivity. All these factors lead to a rise in the power factor, with a maximum value of $\sim 0.42\,mW/K^2\,m$, which is among the best results obtained in this type of materials so far.

Acknowledgements

This research has been supported by the Spanish Ministry of Science and Innovation (Project no. MAT2008–00429) and the Universidad de Zaragoza (Project no. UZ2011-TEC-03). The authors wish to thank the Gobierno de Aragón (Consolidated Research Groups T87 and T12) for financial support and C. Gallego, C. Estepa and J.A. Gomez for their technical assistance. Sh. Rasekh acknowledges a JAE-PreDoc2010 grant from the CSIC.

References

[1] W. Liu, X. Yan, G. Chen, Z. Ren, Recent advances in thermoelectric nanocomposites, Nano Energy 1 (1) (2012) 42–56.
[2] D.M. Rowe, in: D.M. Rowe (Ed.), Thermoelectrics Handbook: Macro to Nano, 1st ed., CRC Press, Boca Raton, FL, 2006, pp. 3–7.
[3] I. Terasaki, Y. Sasago, K. Uchinokura, Large thermoelectric power in $NaCo_2O_4$ single crystals, Physical Review B 56 (20) (1997) 12685–12687.
[4] R. Funahashi, I. Matsubara, H. Ikuta, T. Takeuchi, U. Mizutani, S. Sodeoka, An oxide single crystal with high thermoelectric performance in air, Japanese Journal of Applied Physics 39 (11B) (2000) L1127–L1129.
[5] A.C. Masset, C. Michel, A. Maignan, M. Hervieu, O. Toulemonde, F. Studer, B. Raveau, J. Hejtmanek, Misfit-layered cobaltite with an anisotropic giant magnetoresistance: $Ca_3Co_4O_9$, Physical Review B 62 (1) (2000) 166–175.
[6] H. Leligny, D. Grebille, O. Perez, A.C. Masset, M. Hervieu, B. Raveau, A five-dimensional structural investigation of the misfit layer compound $[Bi_{0.87}SrO_2]_2[CoO_2]_{1.82}$, Acta Crystallographica B 56 (2000) 173–182.
[7] A. Maignan, D. Pelloquin, S. Hebert, Y. Klein, M. Hervieu, Thermoelectric power in misfit cobaltites ceramics: optimization by chemical substitutions, Boletin de la Sociedad Española de Cerámica 45 (3) (2006) 122–125.
[8] W. Kobayashi, S. Hebert, H. Muguerra, D. Grebille, D. Pelloquin, A. Maignan, Thermoelectric properties in the misfit-layered-cobalt oxides [Bi2A2O4] [CoO2]b1/b2 (A=Ca, Sr, Ba, b(1)/b(2)=1.65, 1.82, 1.98) single crystals, in: I. Kim (Ed.), Proceedings of the Twenty-sixth International Conference on Thermoelectrics, ICT 07, Korea, 2008, 117–120.
[9] A. Maignan, S. Hebert, M. Hervieu, C. Michel, D. Pelloquin, D. Khomskii, Magnetoresistance and magnetothermopower properties of Bi/Ca/Co/O and Bi(Pb)/Ca/Co/O misfit layer cobaltites, Journal of Physics: Condensed Matter 15 (17) (2003) 2711–2723.
[10] H. Itahara, C. Xia, J. Sugiyama, T. Tani, Fabrication of textured thermoelectric layered cobaltites with various rock salt-type layers by

using b-$Co(OH)_2$ platelets as reactive templates, Journal of Materials Chemistry 14 (1) (2004) 61–66.
[11] E. Guilmeau, M. Mikami, R. Funahashi, D. Chateigner, Synthesis and thermoelectric properties of $Bi_{2.5}Ca_{2.5}Co_2O_x$ layered cobaltites, Journal of Materials Research 20 (4) (2005) 1002–1008.
[12] W. Shin, N. Murayama, Thermoelectric properties of (Bi,Pb)–Sr–Co–O oxide, Journal of Materials Research 15 (2) (2000) 382–386.
[13] J.G. Noudem, D. Kenfaui, D. Chateigner, M. Gomina, Toward the enhancement of thermoelectric properties of lamellar $Ca_3Co_4O_9$ by edge-free spark plasma texturing, Scripta Materialia 66 (5) (2012) 258–260.
[14] A. Sotelo, E. Guilmeau, M.A. Madre, S. Marinel, J.C. Diez, M. Prevel, Fabrication and properties of textured Bi-based cobaltite thermoelectric rods by zone melting, Journal of the European Ceramic Society 27 (2007) 3697–3700.
[15] H.Q. Liu, X.B. Zhao, T.J. Zhu, Y. Song, F.P. Wang, Thermoelectric properties of Gd, Y co-doped $Ca_3Co_4O_{9+\delta}$, Current Applied Physics 9 (2) (2009) 409–413.
[16] A. Sotelo, Sh. Rasekh, E. Guilmeau, M.A. Madre, M.A. Torres, S. Marinel, J.C. Diez, Improved thermoelectric properties in directionally grown $Bi_2Sr_2Co_{1.8}O_y$ ceramics by Pb for Bi substitution, Materials Research Bulletin 46 (2011) 2537–2542.
[17] A. Sotelo, M.A. Torres, G. Constantinescu, Sh. Rasekh, J.C. Diez, M.A. Madre, Effect of Ag addition on the mechanical and thermoelectric performances of annealed $Bi_2Sr_2Co_{1.8}O_x$ textured ceramics, Journal of the European Ceramic Society 10.1016/j.jeurceramsoc.2012.05.035.
[18] A. Sotelo, M. Mora, M.A. Madre, J.C. Diez, L.A. Angurel, G.F. de la Fuente, Ag distribution in thick Bi-2212 floating zone textured rods, Journal of the European Ceramic Society 25 (2005) 2947–2950.
[19] A. Sotelo, E. Guilmeau, Sh. Rasekh, M.A. Madre, S. Marinel, J.C. Diez, Enhancement of the thermoelectric properties of directionally grown Bi–Ca–Co–O through Pb for Bi substitution, Journal of the European Ceramic Society 30 (2010) 1815–1820.
[20] Z. Gaoke, L. Ying, Y. Xia, W. Yanping, O. Shixi, L. Hangxing, Comparison of synthesis methods, crystal structure and characterisation of strontium cobaltite powders, Materials Chemistry and Physics 99 (1) (2006) 88–95.
[21] A. Sotelo, Sh. Rasekh, M.A. Madre, E. Guilmeau, S. Marinel, J.C. Diez, Solution-based synthesis routes to thermoelectric $Bi_2Ca_2Co_{1.7}O_x$, Journal of the European Ceramic Society 31 (2011) 1763–1769.
[22] A. Sotelo, E. Guilmeau, M.A. Madre, S. Marinel, S. Lemmonier, J.C. Diez, $Bi_2Ca_2Co_{1.7}O_x$ thermoelectric ceramics textured by laser floating zone method, Boletin de la Sociedad Española de Cerámica 47 (4) (2008) 225–228.
[23] J.C. Diez, E. Guilmeau, M.A. Madre, S. Marinel, S. Lemmonier, A. Sotelo, Improvement of $Bi_2Sr_2Co_{1.8}O_x$ thermoelectric properties by laser floating zone texturing, Solid State Ionics 180 (2009) 827–830.
[24] Sh. Rasekh, M.A. Madre, A. Sotelo, E. Guilmeau, S. Marinel, J.C. Diez, Effect of synthetic methods on the thermoelectrical properties of textured $Bi_2Ca_2Co_{1.7}O_x$ ceramics, Boletin de la Sociedad Española de Cerámica 49 (1) (2010) 89–94.
[25] G.F. de la Fuente, J.C. Diez, L.A. Angurel, J.I. Peña, A. Sotelo, R. Navarro, Wavelength dependence in laser floating-zone processing—a case-study with Bi–Sr–Ca–Cu–O superconductors, Advanced Materials 7 (1995) 853–856.
[26] Sh. Rasekh, G. Constantinescu, M.A. Torres, M.A. Madre, J.C. Diez, A. Sotelo, Growth rate effect on microstructure and thermoelectric properties of melt grown $Bi_2Ba_2Co_2O_x$ textured ceramics, Advances in Applied Ceramics. 10.1179/1743676112Y.0000000039.
[27] B. Özkurt, M.A. Madre, A. Sotelo, M.E. Yakinci, B. Özçelik, Relationship between growth speed, microstructure, mechanical and electrical properties in Bi-2212/Ag textured composites, Journal of Superconductivity and Novel Magnetism 25 (4) (2012) 799–804.
[28] M. Kato, Y. Goto, K. Umehara, K. Hirota, I. Terasaki, Synthesis and physical properties of Bi–Sr–Co–oxides with 2D-triangular Co layers intercalated by iodine, Physica B 378–380 (2006) 1062–1063.
[29] D. Mercurio, J.C. Champarnaud-Mesjard, B. Frit, P. Conflant, J.C. Boivin, T. Vogt, Thermal evolution of the crystal-structure of the rhombohedral $Bi_{0.75}Sr_{0.25}O_{1.375}$ phase—a single-crystal neutron-diffraction study, Journal of Solid State Chemistry 112 (1) (1994) 1–8.
[30] G. Becherer, R. Ifland, Über eine präzisionsbestimmung der gitterkonstanten von silber nach dem rückstrahlverfahren, Naturwissenschaft 41 (20) (1954) 471.
[31] M. Mora, A. Sotelo, H. Amaveda, M.A. Madre, J.C. Diez, L.A. Angurel, G.F. de la Fuente, Efecto de la adición de Ag en Bi-2212 texturado mediante laser, Boletin de la Sociedad Española de Cerámica 44 (4) (2005) 199–203.
[32] P. Majewski, A. Sotelo, H. Szillat, S. Kaesche, F. Aldinger, Phase diagram studies in the system Ag–$Bi_2Sr_2CaCu_2O_8$, Physica C 275 (1997) 47–51.
[33] T. Itoh, I. Terasaki, Thermoelectric properties of $Bi_{2.3-x}Pb_xSr_{2.6}Co_2O_y$ single crystals, Japanese Journal of Applied Physics 39 (12A) (2000) 6658–6660.
[34] M. Karppinen, H. Fjellvåg, T. Konno, Y. Morita, T. Motohashi, H. Yamauchi, Evidence for oxygen vacancies in misfit-layered calcium cobalt oxide, $[CoCa_2O_3]_qCoO_2$, Chemistry of Materials 16 (14) (2004) 2790–2793.
[35] W. Koshibae, K. Tsutsui, S. Maekawa, Thermopower in cobalt oxides, Physical Review B 62 (11) (2000) 6869–6872.